

# Learning Multi-frame Visual Representation for Joint Detection and Tracking of Small Objects

Ryota Yoshihashi<sup>1</sup>, Tu Tuan Trinh<sup>1</sup>, Rei Kawakami<sup>1</sup>, Shaodi You<sup>2,3</sup>, Makoto Iida<sup>1</sup>, Takeshi Naemura<sup>1</sup>

<sup>1</sup> The University of Tokyo

<sup>2</sup>Data61-CSIRO

<sup>3</sup>Australian National University

{yoshi, tu, rei, naemura}@hc.ic.i.u-tokyo.ac.jp, iida@ilab.eco.rcast.u-tokyo.ac.jp, shaodi.you@data61.csiro.au

## Abstract

Deep convolutional and recurrent neural networks have delivered significant advancements in object detection and tracking. However, current models handle detection and tracking through separate networks, and deep-learning-based joint detection and tracking has not yet been explored despite its potential benefits to both tasks. In this study, we present an integrated neural model called the *Recurrent Correlational Network* for joint detection and tracking, where the two tasks are performed over multi-frame representation learned through a single, trainable, and end-to-end network. Detection is benefited by the tracker because of the stabilized trajectories and tracking is aided by the enhanced representation afforded by the training of the detector. We show that recently developed convolutional long short-term memory networks can learn multi-frame, multi-task representation, which is useful for both tasks. In experiments, we tackled the detection of small flying objects, such as birds and unmanned aerial vehicles, that can be challenging for single-frame-based detectors. We found that there was consistent improvement in detection performance by the proposed model in comparison with deep single-frame detectors and currently used motion-based detectors.

## Introduction

Motion often enables us to recognize objects, particularly when they appear at a small scale. Visually small objects tend to be blurred and textureless owing to their size; thus, changes in their temporal appearance over a longer time frame may offer richer information than appearance at a glance. As shown in Fig. 1, a bird is much easier to identify when multiple frames are available. For them to be recognized using multiple frames, objects need to be tracked correctly over time, where the tracking should also be assisted by the recognition of objects. Indeed, many studies using classical features have indicated that detection and tracking are complementary tasks (Kalal, Mikolajczyk, and Matas 2010; Breitenstein et al. 2009; Andriluka, Roth, and Schiele 2008; Huang, Wu, and Nevatia 2008).

While deep convolutional networks (convnets) (LeCun et al. 1998), recurrent networks (recurrent nets) (Werbos 1988), and combinations of them have been successful at many tasks, detection and tracking have been tackled separately. Generic object detection in video, yet it is intensively

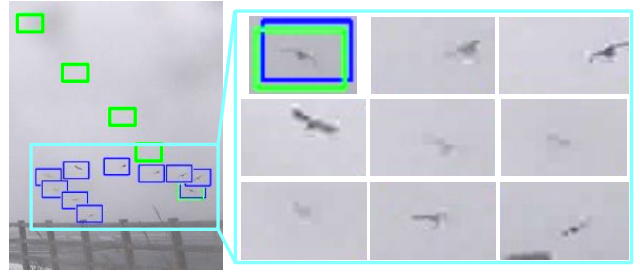


Figure 1: Importance of multi-frame information for recognizing apparently small objects. While visual features in single frames are vague and limited, multi-frame information, including translation and deformation, provides a better clue to recognize birds. The blue boxes are tracked birds by our method that utilizes multi-frame representation for detection, while green boxes by handcrafted-feature-based trackers easily fail to track.

studied and is a closely related problem to ours, the state-of-the-art methods consist of separate detection networks and trackers; namely, most of them are combination of static image-based detectors, tracking of detected boxes, and post-processing for score aggregation. This is partially because static convnets offer sufficiently rich features to localize objects frame by frame in their videos. State-of-the-art trackers were also used to update the benchmark results by replacing classical features with those of convnets (Nam and Han 2016). Recurrent nets, which can learn from time-series data, have also been applied to tracking (Ning et al. 2017; Gordon, Farhadi, and Fox 2017; Milan et al. 2017; Wang, Zhang, and Yi 2017), but have not outperformed convnet-based nets to date. Although recurrent nets, including long short-term memories (LSTMs) (Hochreiter and Schmidhuber 1997) are promising tools for recognition in video that have been successfully applied to video classification (Donahue et al. 2015; Li et al. 2016), extending these video-based networks to object detection and tracking remains largely unexplored.

In this paper, we introduce a recurrent convolutional neural architecture called *Recurrent Correlational Network* that can simultaneously accomplish detection and tracking in video. We utilize convolutional LSTM (ConvLSTM) (Xingjian et al. 2015) to learn discriminative representation of objects in multiple frames to successfully run

the correlation mechanism, a well-accepted tool in tracking, over the hidden state of the pixel-wise memory. The memory can learn local structures in images, which may be lost in fully-connected recurrent layers that most recurrent-net-based trackers rely on (Ning et al. 2017; Gordon, Farhadi, and Fox 2017; Milan et al. 2017; Wang, Zhang, and Yi 2017).

Detection is a class-level task of localization, whereas tracking is an instance-level task that finds target templates in the next frame. Learning shareable representation in both tasks is natural to simplify and reduce the parameters that need to be learned. Thus, our method offers the following advantages over a straightforward combination of detectors and off-the-shelf trackers: First, the learned spatio-temporal representation benefits tracking because it is semantically enhanced by large-scale datasets used to train the detectors. Second, the overall system can be simplified in our joint framework because it does not require separate features or independently trained networks. Our network is fully differentiable and, thus, is end-to-end trainable.

We conducted a large number of experiments with our network on single-class, fully supervised object detection and tracking in videos. Of the variations in the application of object detection, we focused on the surveillance of small flying objects: birds (Trinh et al. 2016) and unmanned aerial vehicles (UAVs) (Rozantsev, Lepetit, and Fua 2017). These detections are challenging for single-frame-based detectors owing to the small apparent size of objects in images that cover a wide area of surveillance. In such situations, visual information from single frames is limited, even for strong convnets. We report the best detection performance in both datasets in comparison with previously published results.

Our contribution is two-fold. First, we show the novel joint framework for object detection and tracking in video. This is the first model to achieve joint detection and tracking with deep learning. ConvLSTM is shown to be capable of learning multi-frame multi-task representations, which is useful for both tasks. Second, we report the best published results in two recently developed flying-object detection datasets. The relevant code and data will be published upon acceptance of this paper.

## Related work

**Joint detection and tracking** The relationship between object detection and tracking is a long-term problem in itself, although it has only been explored with classical tools before deep learning. A representative work is the track-learn detection (TLD) framework (Kalal, Mikolajczyk, and Matas 2010), where the trained detector enables long-term tracking by re-initializing trackers after objects' temporal disappearance. Another typical joint approach involves using detectors as hypothesis samplers for trackers. For example, Andriluka *et al.* introduced a pedestrian detection framework that uses a single-frame part-based detector and shallow unsupervised learning based on temporal consistency (Andriluka, Roth, and Schiele 2008). Tracking by associating detected bounding boxes (Huang, Wu, and Nevatia 2008) is another popular approach. However, recovering undetected objects is challenging in this framework because

tracking is more akin to post-processing following detection than joint detection and tracking.

**Object detection in video** Having achieved significant success in generic object detection in still images, the trend in research began moving toward efficient generic object detection in videos (Girshick et al. 2014; Liu et al. 2016; Redmon and Farhadi 2017). However, methodological changes are not mandatory because still image object detectors are directly applicable to videos through the separate processing of every frame, or coarsely sampled frames. However, some very recent studies have begun improving on detection using video information. Some examples are T-CNNs (Kang et al. 2016; 2017), which use trackers for detection with high confidence, and flow-guided feature aggregation (Zhu et al. 2017), which involves feature-level propagation using optical flow.

**Deep trackers** Recent studies intensively examined convnets and recurrent nets for tracking. Convnet-based trackers learn convolutional layers to acquire rich visual representation, but they do not exploit multi-frame clues. Their localization strategies are diverse. Classification-based approaches (Nam and Han 2016) involve classifying densely sampled candidates into target and non-target regions. This approach yields high-quality localization but the computation is considerably slower than in real time because it needs online retraining. Similarity-learning-based approaches (Li, Kong, and Fu 2017) also handle densely sampled patches but avoid online training by replacing the classifier by learned similarity, and are thus faster. Correlation-based localization is also a faster alternative to region-classification-based approaches, which compute the cross-correlation between convolutional representations of a template and frames (Bertinetto et al. 2016; Valmadre et al. 2017), and has the merit of allowing for the interpretation of correlation heat maps.

Recurrent nets efficiently handle temporal structure in sequences whereas convnets handle spatial structures within single images, and thus have been used in video-understanding tasks. Some recent studies have used recurrent layers and convolutional layers for tracking (Ning et al. 2017; Gordon, Farhadi, and Fox 2017; Milan et al. 2017; Wang, Zhang, and Yi 2017). However, most of them utilize convolutional and recurrent layers as separate layers, and use a fully connected recurrent layer, which may lead to a loss of spatial information. A notable anticipator of our work here is (Ondruska and Posner 2016), where ConvLSTM is used for occlusion handling in simulated robotic sensors.

**Other video recognition techniques** Apart from detection and tracking, the use of recurrent nets has been explored in the wider area of video recognition, such as in video classification and action recognition (Wang, Qiao, and Tang 2015; Weinzaepfel, Harchaoui, and Schmid 2015; Donahue et al. 2015). VideoLSTM (Li et al. 2016) is notable because it uses the idea of inter-frame correlation to recognize actions with attention.

Optical flow (Lucas and Kanade 1981; Horn and Schunck 1981) is an important counterpart of trackers in video processing. While trackers provide object-level stabilization,

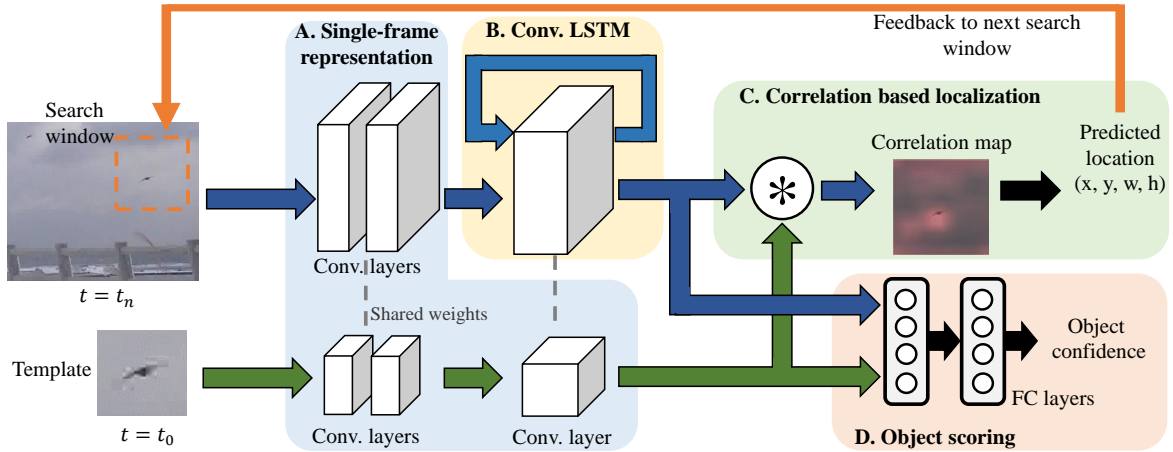


Figure 2: Overview of the proposed network, called *Recurrent Correlation Network* (RCN). It consists of the following four modules: Convolutional layers for single-frame representations (A), ConvLSTM layers for multi-frame representations (B), cross-correlation layers for localization (C), and fully-connected layers for object scoring (D). Green arrows show the information stream from templates, and blue arrows show that from search windows.

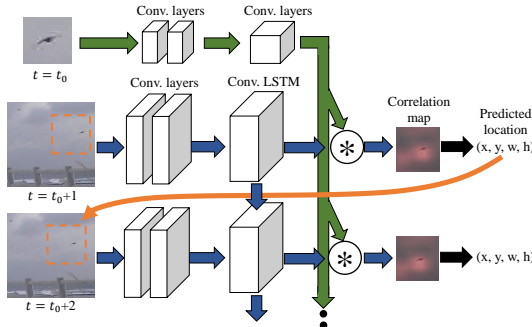


Figure 3: Temporal expansion of the proposed network. The joint tracking is incorporated as a part of feedback in the recurrent cycle.

optical flows provide pixel-level stabilization. Optical-flow-based motion compensation and feature extraction are popular techniques in video recognition with or without deep learning. While we focus on high-level motion stabilization and learning by tracking, we believe flow-based low-level motion handling is orthogonal and complementary to ours.

## Recurrent Correlational Networks

An overview of our network is provided in Fig. 2. To achieve joint detection and tracking, it consists of four modules: convolutional layers, ConvLSTM layers, a cross-correlation layer, and fully connected layers for object scoring. First, convolutional layers model single-frame appearances of target and non-target regions, including other objects and backgrounds (Fig. 2 A). Second, ConvLSTM layers are used to merge single-frame appearances and learn multi-frame motion representation to embed frames into a fixed-dimensional feature map (Fig. 2 B). Third, a cross-correlation layer convolves the single-frame appearance of the template to that of search windows in subsequent frames, and generates correlation maps that are useful for localizing the targets (Fig. 2 C). Finally, the confidence scores of objects are calculated with fully-connected layers based on the multi-frame

representation (Fig. 2 D). The inputs to the network are external object proposal boxes and video frames.

**Correlation-based localization** We utilize a cross-correlation layer for localizing instances (Fig. 2 C), inspired by correlation-based trackers (Bolme et al. 2010; Danelljan et al. 2014; Bertinetto et al. 2016). Cross-correlation is an operation that relates two inputs, and outputs a correlation map that indicates how similar each patch in an image is to another. It is denoted by

$$C(\mathbf{p}) = \mathbf{f} * \mathbf{h} = \sum_{\mathbf{q}} \mathbf{f}(\mathbf{p} + \mathbf{q}) \cdot \mathbf{h}(\mathbf{q}). \quad (1)$$

where  $\mathbf{f}$  and  $\mathbf{h}$  denote the multi-dimensional feature representations of the search window and the template, respectively.  $\mathbf{p}$  is for every pixel's coordinates in the domain of  $\mathbf{f}$ , and  $\mathbf{q}$  is for the same but in the domain of  $\mathbf{h}$ . Two-dimensional (2D) correlation between a target patch and a search window is equivalent to densely comparing the target patch with all possible patches within the search window. The inner product is used here as a similarity measure.

In the context of convolutional neural networks, cross-correlation layers can be considered as a differentiable layer without learnable parameters; namely, a cross-correlation layer is a variant of a usual convolutional one whose kernels are substituted by the output of another layer. Cross-correlation layers are bilinear with respect to two inputs, and thus are differentiable. The computed correlation maps are used to localize the target by

$$\mathbf{p}_{\text{target}} = \text{argmax}_{\mathbf{p}} C(\mathbf{p}). \quad (2)$$

**Convolutional LSTM** To exploit the spatial correlation, the aggregated multi-frame representations need to be in 2D. The recently developed ConvLSTM is well suited to fulfill the requirement as the recurrent module (Fig. 2 B). It is a convolutional counterpart of the well-known LSTM that replaces inner products in the LSTM with convolution. For the

sake of completeness, we show the formulation of ConvLSTM below.

$$\begin{aligned}
i_t &= \sigma(w_{xi} * x_t + w_{hi} * h_{t-1} + b_i) \\
f_t &= \sigma(w_{xf} * x_t + w_{hf} * h_{t-1} + b_f) \\
c_t &= f_t \circ c_{t-1} + i_t \circ \tanh(w_{xc} * x_t + w_{hc} * h_{t-1} + b_c) \\
o_t &= \sigma(w_{xo} * x_t + w_{ho} * h_{t-1} + b_o) \\
h_t &= o_t \circ \tanh(c_t).
\end{aligned} \tag{3}$$

$x_t$  and  $h_t$  denote input and output of the layer at timestep  $t$ , respectively. The states of memory cells are denoted by  $c_t$ .  $i_t$ ,  $f_t$ , and  $o_t$  are called gates, which work for selective memorization. ‘ $\circ$ ’ denotes the Hadamard product.

In our framework, the ConvLSTM module is used for motion feature extraction. It works as a sequence-to-sequence predictor; specifically, it takes series  $(x_1, x_2, x_3, \dots, x_t)$  of single-frame representations whose length is  $t$  as input, and outputs a merged single representation  $h_t$ , at each timestep  $t = 1, 2, 3, \dots, L$ .

While ConvLSTM is effective for video processing, it inherits the complexity of LSTM. The gated recurrent unit (GRU) is a simpler alternative to LSTM that has fewer gates, and is empirically easier to train on some datasets (Chung et al. 2015). A convolutional version of the GRU (ConvGRU) (Siam et al. 2016) is as follows:

$$\begin{aligned}
z_t &= \sigma(w_{xz} * x_t + w_{hz} * h_{t-1} + b_z) \\
r_t &= \sigma(w_{xr} * x_t + w_{hr} * h_{t-1} + b_r) \\
h_t &= z_t \circ h_{t-1} + (1 - z_t) \\
&\circ \tanh(w_{xh} * x_t + w_{hh} * (r_t \circ h_{t-1}) + b_h).
\end{aligned} \tag{4}$$

ConvGRU has only two gates of  $z_t$  and  $r_t$ , while ConvLSTM has three. ConvGRU can also be incorporated into our pipeline, and we provide an empirical comparison between ConvLSTM and ConvGRU for the first time.

**Single-frame representation** Multi-layer convolutional representation is inevitable for natural image recognition, although the original ConvLSTM (Xingjian et al. 2015) does not use non-recurrent convolutional layers for radar-based tasks. Following recent tandem CNN-LSTM models for video recognition (Donahue et al. 2015), we insert non-recurrent convolutional layers before the ConvLSTM layers (Fig. 2 A). Arbitrary types of convolutional architecture can be incorporated here and we should choose the proper ones for each dataset. In experiments, we test two different structures of variant depth.

We need to extract an equivalent representation from the object template for the search windows. We use ConvLSTM, the recurrent connection of which is severed. Specifically, we force the forget gates to be zero and enter zero vectors instead of the previous hidden states. This layer is equivalent to a convolutional layer with  $\tanh$  nonlinearity and sigmoid gates. It shares weights with  $w_{xc}$  in Eq. 3.

**Search window strategy** In object tracking, as the speed of the target objects is physically limited, limiting the area of the search windows, where the correlations are computed, is a natural way to reduce computational cost. We place windows the centers of which are at the previous location of

objects, with a radius  $r = \alpha \max(w, h)$ , where  $w$  and  $h$  are the width and height of the bounding box of the candidate object. We then compute the correlation map for windows around each candidate object. This determination of the search windows is part of a feedback mechanism in the recurrent part, which is shown in Fig. 3. Empirically, we set the size of the search windows to  $\alpha = 1.0$ . The representation extracted from the search windows is also fed into the object scoring part of the network, which yields large field-of-view features and provides contextual information for detection.

**Object scoring** For object detection, the tracked candidates need to be scored according to likeness. We use fully connected (FC) layers for this purpose (Fig. 2 D). We feed both the representation from the templates (green lines in Fig. 2) and the search windows (blue lines in Fig. 2) into the FC layers by concatenation. We used two-layered FC layers here, where the number of dimensions of the hidden vector was 1,000.

We feed the output of each timestep of ConvLSTM into the FC layers and average the scores. In theory, the representation of the final timestep after feeding the last frame of the sequence should provide the maximum information. However, we found that the average scores are more robust in case of tracking failures or the disappearance of the targets.

**Training** Our network is trainable with ordinal gradient-based optimizers in an end-to-end manner because all layers are differentiable. However, we use scheduling techniques to ensure fast convergence. We first train single-frame-based convnets initialized by pre-trained weights in the ILSVRC2012-CLS dataset, the popular and largest generic image dataset. We then fine-tune single-frame convnets in the target datasets (birds and drones) without ConvLSTM. Finally, we add the convolutional LSTM, the correlation layer, and FC layers to the networks and fine-tune them again. For optimization, we use the SGD solver of Caffe (Jia et al. 2014). The total number of iterations was 40,000 and the batch size was five. The original learning rate was 0.01, and was reduced to 0.1 times per 10,000 iterations. The loss was the usual sigmoid cross-entropy. We froze the weights in pre-trained convolutional layers after connecting to the convolutional LSTM to avoid overfitting.

We use pre-computed trajectories and store cropped search windows in the disk during training for efficiency. During the testing phase, the network will observe trajectories estimated by itself, which are different from the ground truths that are used in the training phase. This training scheme is often referred to as teacher forcing (Williams and Zipser 1989). This is intended for efficiency, to reduce disk access by avoiding the re-cropping of the regions of interest out of the 4K-resolution frames during training. Negative samples also need trajectories in training, but we do not have their ground truth trajectories because only the positives are annotated in detection datasets. We use predicted trajectories by a tracker consisting of the final convolutional layers of the pre-trained single-frame convnet and a correlation layer, which are slightly inaccurate but have similar trajectories to our final network.

## Experiments

The main purpose of the experiments was to investigate performance gain owing to joint tracking in detection tasks. We also report the tracking performance of our method and compare it with that of model-free trackers with a variety of features.

We first used a recently constructed video-based bird dataset (Trinh et al. 2016). This dataset involved detecting birds in a wind farm. The resolution was 4K and the frame rate was 30 fps, which made processing the dataset a challenge due to its large volume. The most frequent size of the birds is 55 pixel. The dataset posed the challenges of changes in illumination owing to the weather, changing background patterns owing to clouds, and variation in the appearance of birds due to occlusion and deformation, although the dataset consists of images taken from a fixed-point camera.

We also tested our method on a UAV dataset (Rozantsev, Lepetit, and Fua 2017) to understand whether it can be applied to other types of flying objects. This dataset consisted of 20 sequences of hand-captured videos. It consisted of approximately 8,000 bounding boxes of flying UAVs. All the UAVs in this dataset were multi-copters. We followed the training/testing split provided by the authors of (Rozantsev, Lepetit, and Fua 2017).

**Evaluation metric** To evaluate detection performance, we used the number of false positives per image (FPPI) and the miss rate, considering the dataset (Trinh et al. 2016). Overall performance of each method is evaluated by a scalar, the log average miss rate (MR). These metrics were based on single-image detection, i.e., they were calculated only on given test frames that were sampled discretely. Detection was performed on the given test frames and, for our method, the tracking of candidates was conducted in some of the subsequent frames. We reused the toolkit provided for the Caltech Pedestrian Detection Benchmark (Dollár et al. 2012) to calculate the scores and plot the curves in Fig. 4 (a).

We also report the results of tracking accuracy separately from detection for the bird detection dataset. We conducted one-path evaluation (OPE), tracking by using ground truth bounding boxes given only in the first frame of the snippets without re-initialization, and conducted the re-detection or trajectory fusion in case of objects were lost. To remove very short trajectories to evaluate trackers, we selected ground truth trajectories longer than 90 frames (three seconds in 30 fps) from the annotation of the bird dataset. We plotted the success rates versus overlap thresholds. The curves in Fig. 4 (b) show the proportion of the estimated bounding boxes whose overlaps with the ground truths were higher than the thresholds.

**Object proposals** We used a different strategy for each dataset to generate object proposals for pre-processing. In the bird dataset, we extracted the moving object by background subtraction (Zivkovic 2004). The extracted regions were provided by the authors with the dataset; therefore, we could compare the networks fairly, regardless the hyperparameters and the detailed tuning of background subtraction.

In the UAV dataset, we used the HOG3D-based sliding window detector provided by the authors of (Rozantsev, Lepetit, and Fua 2017).

**Compared methods** *RCN (Alex)* and *RCN (VGG16)* are two implementations of the proposed method using the ImageNet-pretrained convolutional layers from AlexNet (Krizhevsky, Sutskever, and Hinton 2012) and VGG16Net (Simonyan and Zisserman 2015). *HOG tracker+AlexNet* and *HOG tracker+LRCN* are baselines for the bird dataset provided by (Trinh et al. 2016). The former is a combination of the HOG-based (Dalal and Triggs 2005) discriminative tracker DSST (Danelljan et al. 2014; 2017) and convnets that classify the tracked candidates into positives and negatives. The latter is a combination of DSST and the CNN-LSTM tandem model (Donahue et al. 2015). They use five frames following the test frames, and our method also used the same number of frames in detection evaluation for fair comparison.

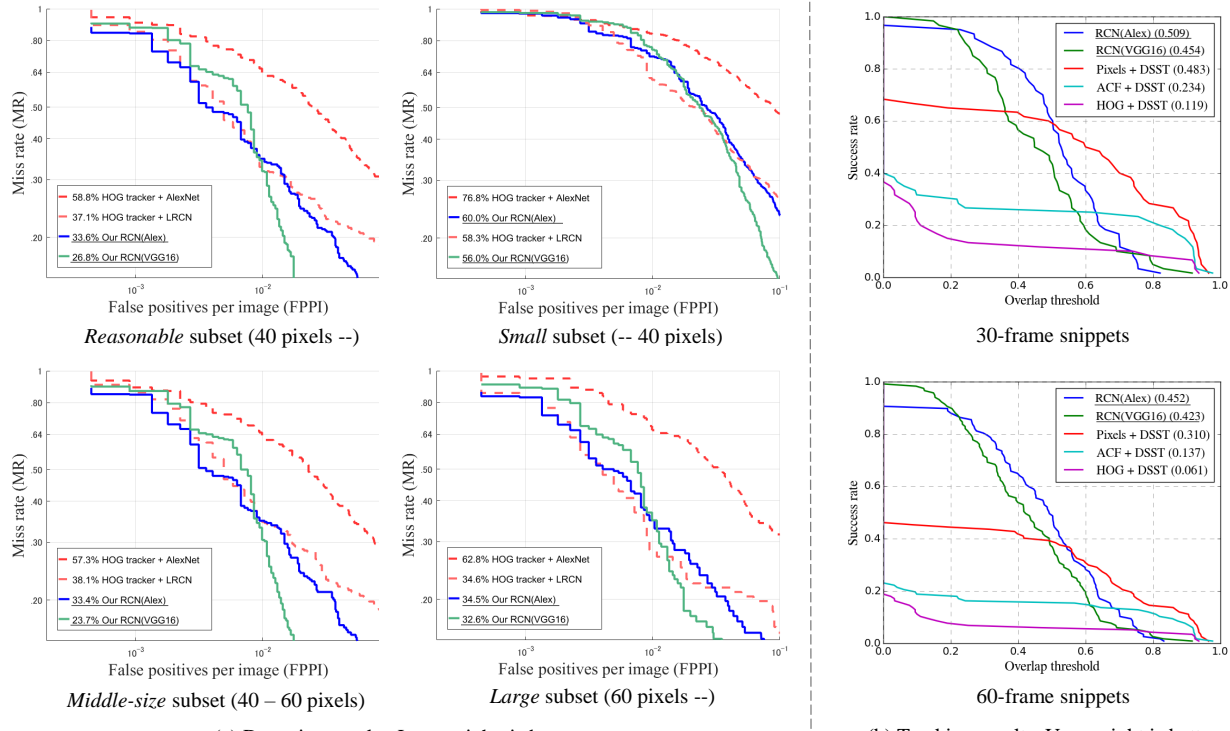
In evaluating tracking performance, we included other combinations of the DSST and hand-crafted features for further analysis. *HOG+DSST* is the original version in (Danelljan et al. 2014). *ACF+DSST* replaced the classical HOG with more discriminative aggregated channel features (Dollár et al. 2014). The ACF is similar to HOG, but is more powerful because of additional gradient magnitude and LUV channels for orientation histograms. *Pixel+DSST* is a simplified version that uses RGB values of raw pixels instead of gradient-based features.

**Result** The results of detection on the bird dataset are shown in Fig. 4 (a). We report the curves for four subsets of the test set, which consists of birds of different sizes, namely *reasonable* (over 40 pixels square), *small* (smaller than 40 pixels square), *middle sized* (40–60 pixels square), and *large* (over 60 pixels square).

In all subsets, the proposed *RCN (VGG16)* showed the smallest average miss rate (MR) of the tested detectors. The improvements by ours are -10.3 percentage points in *Reasonable*, -2.3 percentage points in *Small*, -14.4 in *Middle-size*, and -2.0 percentage points in *Large* subset, in comparison to the previous best published method *HOG tracker+LRCN*.

Comparison of *HOG tracker+LRCN* and proposed *RCN (Alex)* is also important, because these share the same convolutional architecture. Our *RCN (Alex)* performed better in all of the subset except *Small* subset, without deepening the network. The margins are -3.5 percentage points in *Reasonable*, -4.7 percentage points in *Middle-size* subset, and -0.1 percentage points in *Large* subset. The examples of the test frames and results are shown in Fig. 5 and more can be seen in the supplementary material.

A comparison of *RCN (Alex)* and *RCN (VGG16)* provides an interesting insight. *RCN (Alex)* is more robust against smaller FPPI in spite of lower average performance than *RCN (VGG16)*. *RCN (Alex)* showed a smaller MR than *RCN (VGG16)* when the FPPI was lower than  $10^{-2}$ . The possible reason is that a deeper network is less generalizable because of many parameters; thus, it may miss-classify new negatives more often in the test set than the shallower one.



(a) Detection results. Lower right is better.

Figure 4: Resulting curves of detection and tracking. (a) The detection results. Our RCN (VGG16) outperformed all of the other methods by deeper convolutional layers, and our RCN (Alex) outperformed the previous method with the same depth of convolutional layers in three subsets. The subsets are separated by sizes of birds. (b) Tracking results. The proposed methods outperformed DSST trackers with various handcrafted features.

The results of tracking on the bird dataset are shown in Fig. 4 (b). We found gradient-based features were inefficient for this dataset. HOG-based DSST easily missed the target even in 30-frame short tracking (but this was already longer than in (Trinh et al. 2016) for detection). We assume this was because of the way the HOG normalizes the gradients, which might render it over-sensitive to low-contrast but complex background patterns, like clouds. We found that replacing HOG with ACF and utilizing gradient magnitudes and LUV values benefited the DSST on the bird dataset. However, the simpler pixel-DSST outperformed the ACF-DSST by large margins.

The trajectories provided by our network were more robust than all DSST variations tested. This shows that the representation learned through detection tasks also work for tracking better than hand-crafted gradient features. It also worth noting that our trajectories were less accurate than those obtained through the feature-based DSSTs when they did not miss the target. When higher bounding-box overlaps than 0.6 were needed, the success rates were smaller than those of the DSSTs both for 30- and 60-frame tracking. This is because our network used the correlation involving pooled representation, the resolution of which was 32 times smaller than that of the original images. The trade-off between robustness and localization accuracy has to be tuned depending on applications. Tracking results can be seen in the supplementary material.

The resulting ROC curves of drone detection are shown

in Fig. 6. We report the results of a shallower AlexNet-based version of our RCN, because of the size of training data. We also show the curve yielded by AlexNet after single-frame pre-training without LSTM and tracking, which we refer to *Our AlexNet only*. This simple implementation slightly outperformed the baseline in (Rozantsev, Lepetit, and Fua 2017) without auxiliary multi-frame information by tracking or motion compensation. Our network was different in that it was deeper and larger, and had been pre-trained in ImageNet. It is interesting that pre-training in ImageNet classification is useful even in this domain of small, grayscale UAV detection. The ConvLSTM and joint tracking consistently improved in detection performance (-4.3 percentage points). However, the performance gain was smaller than that on the bird dataset. This seemed to have been because motion information in the UAV dataset was limited because the objects are rigid, in contrast to articulated deformation in birds. Examples of the results are shown in Fig. 7.

**Hyperparameters and ablation** For further analysis, we report the fluctuation in performance following different settings of the model structures and hyperparameters. We investigated the following factors: 1) Kernel size in ConvLSTM, 2) ConvGRU vs. ConvLSTM, 3) w/o tracking, and 4) w/o ConvLSTM. Kernel size controls the area in the images to be seen in a memory cell. We also observed the effect of simplifying ConvLSTM to ConvGRU. Third, we removed the joint tracker to observe how useful multi-frame information was without stabilization. Finally, we removed the

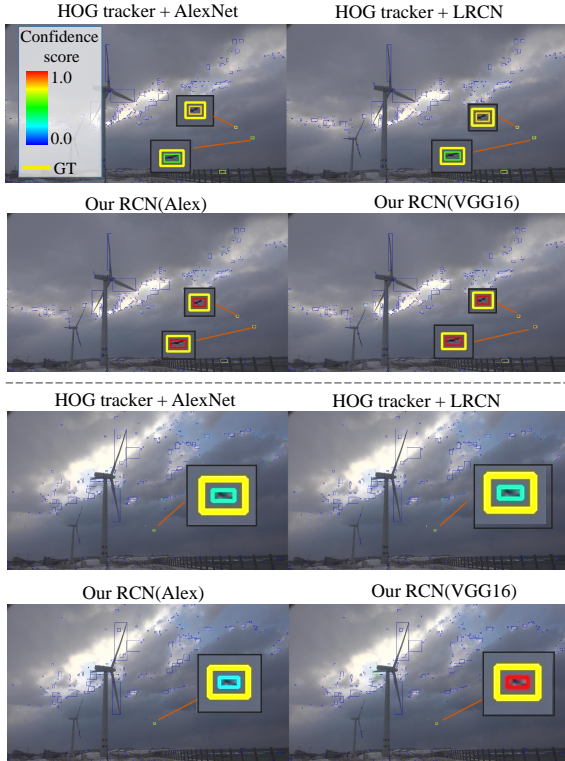


Figure 5: Example frames of the results of detection on the bird dataset (Trinh et al. 2016). The bolder yellow boxes show ground truths, enlarged to avoid overlapping and keep them visible. The confidence score of vague birds are increased by our RCN detector.

recurrent part and apply it as a single-frame detector. The results are summarized in Table 1. All results were in the *reasonable* subset of the bird dataset. The best kernel size was  $k = 3$  in RCN (Alex). Larger and smaller kernels adversely affected performance (+0.011 and +0.010 MR). The performance of the ConvGRU was slightly worse than that of ConvLSTM (+0.003 MR), possibly because the input was pre-processed by convolutional layers and the burden on the recurrent part was smaller. Finally, the lack of stabilization or recurrent parts showed a critical degradation in performance (+0.053 and +0.064 MR).

## Conclusion

In this paper, we introduced the *Recurrent Correlation Network*, a novel joint detection and tracking framework that uses correlation and convolutional LSTMs in a convnet-based end-to-end learnable pipeline. In experiments, we tackled with two recently developed datasets consisting of images of small flying objects, where the use of multi-frame information is inevitable due to poor per-frame visual information. The results showed that in such situations, multi-frame information exploited by the ConvLSTM and tracking-based motion compensation yields better detection performance. In future work, we will try to extend the framework to more generic multi-class object detection in videos.

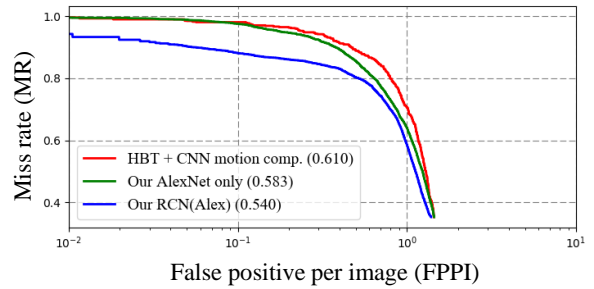
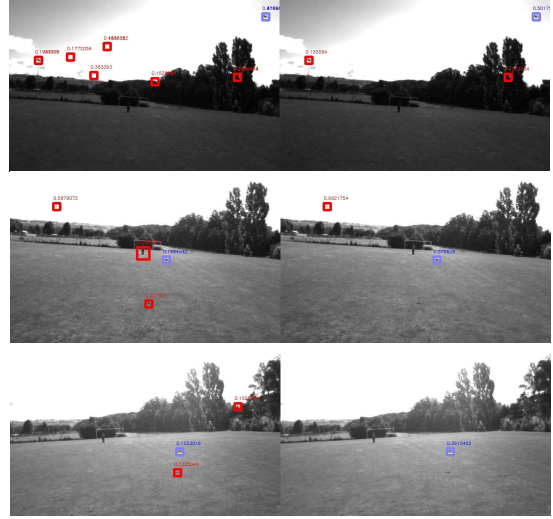


Figure 6: Detection results on the UAV dataset (Rozantsev, Lepetit, and Fua 2017). RCN performed the best.



HBT + CNN motion compensation (Rozantsev, Lepetit, and Fua 2017) Proposed method

Figure 7: Sample frames of detection results on the UAV dataset (Rozantsev, Lepetit, and Fua 2017). The blue boxes show correct detection and the red ones show misdetection. Our method caused fewer misdetection when the detectors thresholds are set to give roughly same FPPI.

		MR	diff.
RCN(Alex)	$k = 1$	0.346	+ 0.010
	$k = 3$	0.336	0 (baseline)
	$k = 5$	0.347	+ 0.011
RCN(VGG16)	$k = 3$	0.268	0 (baseline)
	ConvGRU $k = 3$	0.271	+ 0.003
	w/o tracking	0.321	+ 0.053
	w/o ConvLSTM	0.332	+ 0.064

Table 1: Performance differences by varying models and parameters. MR represents the log-average miss rate in the *reasonable* subset of the bird dataset, and diff. represents its difference from the baseline.  $k$  denotes the kernel size of the ConvLSTM.

## References

Andriluka, M.; Roth, S.; and Schiele, B. 2008. People-tracking-by-detection and people-detection-by-tracking. In *CVPR*, 1–8.

Bertinetto, L.; Valmadre, J.; Henriques, J. F.; Vedaldi, A.; and Torr, P. H. 2016. Fully-convolutional siamese networks for object tracking. In *ECCVW*, 850–865.

Bolme, D. S.; Beveridge, J. R.; Draper, B. A.; and Lui, Y. M. 2010. Visual object tracking using adaptive correlation filters. In *CVPR*, 2544–2550. IEEE.

Breitenstein, M. D.; Reichlin, F.; Leibe, B.; Koller-Meier, E.; and Van Gool, L. 2009. Robust tracking-by-detection using a detector confidence particle filter. In *ICCV*, 1515–1522. IEEE.

Chung, J.; Gulcehre, C.; Cho, K.; and Bengio, Y. 2015. Gated feedback recurrent neural networks. In *ICML*, 2067–2075.

Dalal, N., and Triggs, B. 2005. Histograms of oriented gradients for human detection. In *CVPR*, volume 1, 886–893. IEEE.

Danelljan, M.; Häger, G.; Khan, F.; and Felsberg, M. 2014. Accurate scale estimation for robust visual tracking. In *BMVC*.

Danelljan, M.; Häger, G.; Khan, F. S.; and Felsberg, M. 2017. Discriminative scale space tracking. *PAMI* 39(8):1561–1575.

Dollár, P.; Wojek, C.; Schiele, B.; and Perona, P. 2012. Pedestrian detection: An evaluation of the state of the art. *PAMI* 34(4):743–761.

Dollár, P.; Appel, R.; Belongie, S.; and Perona, P. 2014. Fast feature pyramids for object detection. *PAMI* 36(8):1532–1545.

Donahue, J.; Anne Hendricks, L.; Guadarrama, S.; Rohrbach, M.; Venugopalan, S.; Saenko, K.; and Darrell, T. 2015. Long-term recurrent convolutional networks for visual recognition and description. In *CVPR*, 2625–2634.

Girshick, R.; Donahue, J.; Darrell, T.; and Malik, J. 2014. Rich feature hierarchies for accurate object detection and semantic segmentation. In *Proceedings of the IEEE conference on computer vision and pattern recognition*, 580–587.

Gordon, D.; Farhadi, A.; and Fox, D. 2017. Re3: Real-time recurrent regression networks for object tracking. *arXiv preprint arXiv:1705.06368*.

Hochreiter, S., and Schmidhuber, J. 1997. Long short-term memory. *Neural computation* 9(8):1735–1780.

Horn, B. K., and Schunck, B. G. 1981. Determining optical flow. *Artificial intelligence* 17(1-3):185–203.

Huang, C.; Wu, B.; and Nevatia, R. 2008. Robust object tracking by hierarchical association of detection responses. In *ECCV*, 788–801. Springer.

Jia, Y.; Shelhamer, E.; Donahue, J.; Karayev, S.; Long, J.; Girshick, R.; Guadarrama, S.; and Darrell, T. 2014. Caffe: Convolutional architecture for fast feature embedding. In *ACMMM*, 675–678.

Kalal, Z.; Mikolajczyk, K.; and Matas, J. 2010. Tracking-learning-detection. *PAMI* 34(7):1409–1422.

Kang, K.; Ouyang, W.; Li, H.; and Wang, X. 2016. Object detection from video tubelets with convolutional neural networks. In *CVPR*.

Kang, K.; Li, H.; Yan, J.; Zeng, X.; Yang, B.; Xiao, T.; Zhang, C.; Wang, Z.; Wang, R.; Wang, X.; et al. 2017. T-CNN: Tubelets with convolutional neural networks for object detection from videos. *IEEE Transactions on Circuits and Systems for Video Technology*.

Krizhevsky, A.; Sutskever, I.; and Hinton, G. E. 2012. Imagenet classification with deep convolutional neural networks. In *NIPS*, 1097–1105.

LeCun, Y.; Bottou, L.; Bengio, Y.; and Haffner, P. 1998. Gradient-based learning applied to document recognition. *Proceedings of the IEEE* 86(11):2278–2324.

Li, Z.; Gavves, E.; Jain, M.; and Snoek, C. G. 2016. VideoLSTM colves, attends and flows for action recognition. *arXiv preprint arXiv:1607.01794*.

Li, K.; Kong, Y.; and Fu, Y. 2017. Multi-stream deep similarity learning networks for visual tracking. *IJCAI*.

Liu, W.; Anguelov, D.; Erhan, D.; Szegedy, C.; Reed, S.; Fu, C.-Y.; and Berg, A. C. 2016. SSD: Single shot multibox detector. In *ECCV*, 21–37. Springer.

Lucas, B. D., and Kanade, T. 1981. An iterative image registration technique with an application to stereo vision. In *IJCAI*, 674–679.

Milan, A.; Rezatofighi, S. H.; Dick, A. R.; Reid, I. D.; and Schindler, K. 2017. Online multi-target tracking using recurrent neural networks. In *AAAI*, 4225–4232.

Nam, H., and Han, B. 2016. Learning multi-domain convolutional neural networks for visual tracking. In *CVPR*, 4293–4302.

Ning, G.; Zhang, Z.; Huang, C.; He, Z.; Ren, X.; and Wang, H. 2017. Spatially supervised recurrent convolutional neural networks for visual object tracking. In *IEEE International Symposium on Circuits and Systems*.

Ondruska, P., and Posner, I. 2016. Deep tracking: Seeing beyond seeing using recurrent neural networks. In *AAAI*.

Redmon, J., and Farhadi, A. 2017. YOLO9000: Better, faster, stronger. In *CVPR*.

Rozantsev, A.; Lepetit, V.; and Fua, P. 2017. Detecting flying objects using a single moving camera. *PAMI* 39(5):879–892.

Siam, M.; Valipour, S.; Jagersand, M.; and Ray, N. 2016. Convolutional gated recurrent networks for video segmentation. *arXiv preprint arXiv:1611.05435*.

Simonyan, K., and Zisserman, A. 2015. Very deep convolutional networks for large-scale image recognition. In *ICLR*.

Trinh, T. T.; Yoshihashi, R.; Kawakami, R.; Iida, M.; and Naemura, T. 2016. Bird detection near wind turbines from high-resolution video using lstm networks. In *World Wind Energy Conference (WWEC)*.

Valmadre, J.; Bertinetto, L.; Henriques, J. F.; Vedaldi, A.; and Torr, P. H. 2017. End-to-end representation learning for correlation filter based tracking. *CVPR*.

Wang, L.; Qiao, Y.; and Tang, X. 2015. Action recognition with trajectory-pooled deep- descriptors. In *CVPR*, 4305–4314.

Wang, L.; Zhang, L.; and Yi, Z. 2017. Trajectory predictor by using recurrent neural networks in visual tracking. *IEEE Transactions on Cybernetics*.

Weinzaepfel, P.; Harchaoui, Z.; and Schmid, C. 2015. Learning to track for spatio-temporal action localization. In *Proceedings of the IEEE International Conference on Computer Vision*, 3164–3172.

Werbos, P. J. 1988. Generalization of backpropagation with application to a recurrent gas market model. *Neural networks* 1(4):339–356.

Williams, R. J., and Zipser, D. 1989. A learning algorithm for continually running fully recurrent neural networks. *Neural computation* 1(2):270–280.

Xingjian, S.; Chen, Z.; Wang, H.; Yeung, D.-Y.; Wong, W.-K.; and Woo, W.-c. 2015. Convolutional LSTM network: A machine learning approach for precipitation nowcasting. In *NIPS*, 802–810.

Zhu, X.; Wang, Y.; Dai, J.; Yuan, L.; and Wei, Y. 2017. Flow-guided feature aggregation for video object detection. In *ICCV*.

Zivkovic, Z. 2004. Improved adaptive gaussian mixture model for background subtraction. volume 2, 28–31. IEEE.